

# **Pressures at the base of dry and dense flows of angular rock fragments in 3-D discrete element modeling: Scaling of basal pressure fluctuations versus grain size, flow volume and channel width**

B. Cagnoli<sup>1</sup>, and A. Piersanti<sup>2</sup>

<sup>1</sup>Istituto Nazionale di Geofisica e Vulcanologia, Via Donato Creti 12, 40128 Bologna, Italy.

<sup>2</sup>Istituto Nazionale di Geofisica e Vulcanologia, Via di Vigna Murata 605, 00143 Rome, Italy.

## **Abstract**

We simulate granular flows of angular rock fragments by means of 3D discrete element modeling to study the basal pressures that these flows exert on the subsurface. The flows travel on a concave upward chute reproducing a channel on the flanks of a mountain or a volcano. These flows pertain to dry rock avalanches and pyroclastic flows. The pressure data demonstrate the validity of a linear relation between two scaling parameters. The first parameter is a scaled basal pressure deviation that represents a scaled particle agitation. Particle agitation inside the flows generates the basal friction that governs the mobility of geophysical flows in nature. The second scaling parameter contains grain size, flow volume and channel width. This second parameter is equivalent to the product of the reciprocal of characteristic numbers of fragments, so that, since they are dimensionless, it is valid at any scale, either in the laboratory or and in nature.

## **1. Introduction**

In this paper we study by means of a 3-D discrete element modeling the basal pressures exerted on the subsurface by granular flows of angular rock fragments. We proved that this modeling predicts correctly the relative mobility of laboratory granular flows of angular rock fragments with different grain sizes and different flow volumes (Cagnoli and Romano, 2012a; Cagnoli and Piersanti, 2015). In the new set of numerical simulations examined here, besides the grain size and flow volume of the granular flows, we vary also the values of the channel width. By varying simultaneously the values of these three quantities, it is possible to demonstrate the validity of a dimensionless scaling parameter that the scaled basal pressure fluctuation is proportional to. This was not possible with the laboratory data because the values of the channel width did not vary in the laboratory experiments (Cagnoli and Romano, 2012b).

The dry geophysical flows of rock fragments our research pertains to include rock avalanches (e.g., Zhang and Yin, 2013) and dense pyroclastic flow, such as block-and-ash flows (e.g., Saucedo et al., 2002). These flows are among the most dangerous natural phenomena because of their long travel distances and their destructive capability. Basal pressures are important because they generate the basal friction that controls the mobility of geophysical flows and, therefore, the associated natural hazards. The basal flow interactions are responsible for entrainment of new material when traveling (Yohannes et al., 2012), which also affects the flow runouts (Kang et al., 2016). The mobility of the centre of mass of the flows whose basal pressures we examine in this paper was analysed by Cagnoli and Piersanti (2017).

Our numerical simulations calculate for each granular flow the total basal forces as well as their components that are normal, parallel and transversal with respect to the basal channel surface and the flow direction. This differs from our laboratory experiments, where a load cell allowed the measurement of only the component of the basal forces normal to the slope surface (Cagnoli and Romano, 2012b). We know that these forces are due to particle collisions because, in the laboratory experiments, the load cell plate was small with respect to the grain size so that single particle collisions were detected (Cagnoli and Romano, 2012b). We believe that particle collisions affect importantly the basal interactions of geophysical flows in nature (e.g., McCoy et al., 2013).

Here we study particle agitation to understand how energy is dissipated by granular flows. We define particle agitation as any departure of the particle motion from the downhill direction as a result of the frictional and collisional interaction of the particles with the asperities of the subsurface and the sidewalls. We measure particle agitation as the average pressure deviation from the mean pressure of the basal pressure values. The larger the particle agitation, the larger the energy dissipation of the granular flows and the smaller their mobility (Cagnoli and Romano, 2012a; Cagnoli and Piersanti, 2015).

## 2. Method

### 2.1. Features of Particles and Channels in the Numerical Simulations

Our numerical simulations are carried out by using a 3-D discrete element modeling of dry granular flows of angular rock fragments. These flows travel down channels that have been generated by a CAD software (Rhinoceros). The channels consist of a straight upper ramp and a curved chute (Fig. 1). The longitudinal profile of all curved chutes has the shape of a hyperbolic sine:

$$z=0.3-0.085 \operatorname{arcsinh}(11.765x), \quad (1)$$

whose variables are in meters. The horizontal length of the curved chutes is 1.4 m. Upper ramps and curved chutes have trapezoidal cross sections with different width  $w$ . This width  $w$  is measured at the base of the sidewalls (see inset in Fig. 1). In this paper, the lateral side inclination  $\theta$  is always equal to  $27^\circ$ , whereas we use four channels with a different width  $w$  each (6, 10, 16 and 26 mm, respectively).

The granular material is positioned behind a gate that is removed in a direction perpendicular to that of the slope to release the particles. The gate is located 22.3 cm along the upper ramp (this distance is measured upward from the base of the ramp). Since the initial degree of compaction of the granular material behind the gate before release affects significantly the features of a granular flow as suggested by its different mobility (Cagnoli and Piersanti, 2015), in all our numerical simulations we adopt the same initial bulk density ( $721 \pm 14 \text{ kg/m}^3$ ). After the gate removal, the granular material accelerates down the slope, reaches a maximum speed and then it decelerates and stops. Fig. 2 illustrates a granular flow imaged from above during its descent along the channel. The final deposit consists of that of the granular flow proper (whose particles interact among

themselves when traveling) and a spray of isolated more distal particles (which do not interact among themselves when traveling). In our paper we study the flow proper which is the denser portion of the moving granular mass.

The granular flows consist of particles with a cubic, half a cubic and a quarter of a cubic shape (Fig. 3). The proportions of these particle shapes are 38%, 22% and 40% of the flow mass, respectively. Since flows with different proportions of particles shapes dissipate different amount of energy per unit of travel distance (Cagnoli and Piersanti, 2015), these proportions are held constant in all numerical simulations. The grain size is measured as the length of the longer edges of geometrically similar polyhedrons (Fig. 3). These longer edges can be 1, 1.5 and 2 mm long. Only one grain size is used in each simulation. Table 1 illustrates the combinations adopted in the numerical simulations of the values of the channel width  $w$ , the grain size  $\delta$  and the total granular flow mass. These flow masses have been computed by multiplying the particle density ( $2700 \text{ kg/m}^3$ ) by the sum of the volumes of the polyhedrons of the flows proper.

Our 3-D discrete element modeling has been carried out by means of the software EDEM developed by DEM Solutions. EDEM uses the mass, volume and moment of inertia of the polyhedron we have chosen, whereas it estimates impact forces during particle collisions as a function of the overlapping of sets of spheres inscribed within the polyhedrons (Fig. 3). Cagnoli and Piersanti (2015) showed that the polyhedrons in Fig. 3 model successfully the relative mobility of laboratory flows of angular rock fragments. Our simulations thus pertain to angular fragments, whose frictional properties differ from those of spherical particles (Lambe and Whitman, 1969; Abe and Mair, 2009).

Table 2 shows the values of the physical properties of particles, channels and gates used in the numerical simulations. Table 3 shows the values of the properties that affect particle-particle, particle-channel and particle-gate interactions. These values indicate that we are simulating flows of rock fragments that travel on a subsurface made of soil (Peng, 2000). The gates are made of aluminium. The friction exerted by the gate on the granular material is small to prevent the particles from being disturbed when the gates are removed.

The EDEM contact model that governs particle-particle and particle-boundary interactions is based on the Hertzian contact theory and on the Mindlin-Deresiewicz work (Hertz, 1882; Mindlin, 1949; Mindlin and Deresiewicz, 1953). The equations of this contact model are illustrated in the paper by Cagnoli and Piersanti (2015). The values shown in Tables 2 and 3 are the same as those adopted in the numerical simulations by Cagnoli and Piersanti (2015) because, with these values, it has been possible to obtain the same relative mobility of the different flows as that observed in the laboratory by Cagnoli and Romano (2012a).

## *2.2 Basal Pressure Data*

The EDEM software computes the forces exerted by the granular flows on the channels. In the central basal surface of each channel, we select three square

measurement areas whose sides are equal to the channel width  $w$  (they, thus, stretch from the base of one inclined sidewall to the other). The highest elevation measurement area is called area one and it is located on the curved chute, 6.8 cm below the low end of the ramp. The intermediate elevation measurement area is called area two and it is located on the curved chute, 13.6 cm below the low end of the ramp. The lowest elevation measurement area is called area three and it is located on the curved chute, 20.4 cm below the low end of the ramp. These distances are measured along the curved chute. The area one (the most proximal) is closer to the gates, whereas the area three (the most distal) is closer to the final deposits.

The total basal forces exerted by the flows on the three measurement areas are resolved into their components along the normal, parallel and transversal directions with respect to the channel basal surface and the downhill direction. We then compute the mean pressures exerted by the entire granular flows during their travel time on the three measurement areas along these normal, parallel and transversal directions. All the normal pressures experienced by the channel point toward its basal surface, whereas the parallel and the transversal pressures can point either upslope or downslope and either rightward or leftward, respectively.

Most of the slope parallel components of pressure have a positive sign which signifies that this stress felt by the channel surface as result of a downslope moving flow points downslope. However, a few have a negative sign. Since these pressures are due to particle collisions that dissipate energy, we are interested here in their magnitude, so that, in section 3.1, we use the absolute value of the parallel pressures to compute parameter  $D$ . This choice is correct because we are not dealing with a single sliding object (a brick for example) where the slope-parallel stresses experienced by the slope can only point downhill. We are dealing with particle collisions and some of them can be directed backward with respect to flow direction.

Also the transversal pressures can have either a positive or a negative sign. Since these pressures are due to particle collisions that dissipate energy, we are again interested in their magnitude, so that, in section 3.1, we use the absolute value of the transversal pressures to compute parameter  $D$ . This again is the correct choice because we are dealing with particle collisions which, in a granular flow, can be directed either leftward or rightward along the direction transversal to that of flow motion.

### **3. Scaling Parameters**

#### *3.1. Normalized Basal Pressure Fluctuation $D$*

The data set of the basal pressures exerted on each measurement area by each granular flow consists of a time series of pressure values  $P_i$  with a time step equal to 0.01 sec. Fig. 4 shows an example of a time series of total pressure values. We discard data points at the extremities of each time series when they are separated by the rest of the flow signal by more than one zero-pressure data point. This is meant to discard the pressures exerted by the saltating particles that travel at the front and at the back of the dense flows proper

(Fig. 2). This is a conservative criterion, however, because, by applying it, the time series are retained in almost their entirety.

For each time series we compute the average pressure deviation  $\Delta P$  from their mean pressure  $\bar{P}$ :

$$\Delta P = \sqrt{\langle (P_i - \bar{P})^2 \rangle}, \quad (2)$$

where the angle brackets symbolise the average for each flow signal. We then scale  $\Delta P$  by the mean pressure to obtain

$$D = \frac{\Delta P}{\bar{P}}. \quad (3)$$

The mean pressure  $\bar{P}$  is the average pressure exerted by each flow during its total travel time on the measurement area. Therefore, this average takes into consideration also the zero-pressure data points that can occur between collisions inside the time series. The larger  $\Delta P$ , the larger the number of pressure values that are more different from the mean pressure and, for this reason,  $\Delta P$  represents particle agitation at the base of the flows. Parameter  $D$ , instead, represents a scaled particle agitation at the base of the flows. We calculate four different  $D$  values for each measurement area. These  $D$  values refer to the total, normal, parallel and transversal pressures, respectively.

### 3.2. Scaling Parameter $\psi$

There are several variables that govern the value of pressure deviation  $D$  including those in the following equation:

$$D = f_1(\delta, V, w, s, g, \rho_s, \rho_f, \eta, \phi, e, i, \theta), \quad (4)$$

where  $\delta$  is the mean grain size,  $V$  is the flow volume,  $w$  is the channel width,  $s$  is the initial flow speed,  $g$  is the acceleration of gravity,  $\rho_s$  is the density of the solid grains,  $\rho_f$  is the density of the intergranular fluid,  $\eta$  is the dynamic viscosity of the intergranular fluid,  $\phi$  is the angle of internal friction of the rock fragments,  $e$  is coefficient of restitution of the rock material,  $i$  is the average height (i.e., the roughness) of the chute surface asperities and  $\theta$  is the inclination of the sidewalls. However, in our numerical simulations, the last nine independent variables have values that do not vary because 1) the initial speed of our flows is always zero, 2) gravity does not change, 3) the properties of the rock material are constant, 4) there is no intergranular fluid and 5) the roughness of the channel surfaces is always the same. Also the side inclination  $\theta$  does not vary in this paper and this is important because granular flows in channels with different  $\theta$  values have different features (Cagnoli and Piersanti, 2017). Therefore, Eq. (4) reduces to:

$$D = f_2(\delta, V, w). \quad (5)$$

According to the Buckingham Pi theorem (e.g., Dym, 2004), an equation with four quantities and one fundamental dimension (length) is equivalent to a functional relation between three dimensionless parameters. Since the grain size  $\delta$  is the pertinent length scale for the grain-scale mechanics that generates the stresses (Iverson et al., 2010), we use  $\delta$  to scale the independent variables in Eq. (5), which is thus replaced by

$$D = f_3\left(\frac{V^{1/3}}{\delta}, \frac{w}{\delta}\right). \quad (6)$$

Our simulations show that the basal pressure fluctuation  $D$  is proportional to parameter  $\psi$  which is equal to the product of the reciprocal of the two independent dimensionless quantities of Eq. (6):

$$D = p\psi + q, \quad (7)$$

where

$$\psi = \frac{\delta^2}{V^{1/3}w} \quad (8)$$

and  $p$  and  $q$  are coefficients. Parameter  $\psi$  can thus be written as

$$\psi = \frac{1}{\Gamma} \frac{1}{\Pi} \quad (9)$$

where

$$\Gamma = \frac{V^{1/3}}{\delta} \quad (10)$$

and

$$\Omega = \frac{w}{\delta}. \quad (11)$$

The dimensionless quantity  $\Gamma$  is an increasing function of the total number of particles in the granular flow because it is equivalent to  $V/\delta^3$ . The dimensionless quantity  $\Omega$  is an increasing function of the number of particles which fits the channel width along the transversal direction. Eq. (7) shows that pressure fluctuation  $D$  is inversely proportional to these two characteristics number of particles.

### 3.3. Apparent Basal Friction Coefficients

The basal pressure data we study in this paper enable the calculation of the following apparent coefficient of friction:

$$\mu_B = \frac{\bar{P}_P}{\bar{P}_N}, \quad (12)$$

where  $\bar{P}_P$  is the mean parallel pressure and  $\bar{P}_N$  is the mean normal pressure. Eq. (12) is Coulomb's law. Parameter  $\mu_B$  is computed for areas one, two and three.

In our previous studies, both in laboratory experiments (Cagnoli and Romano, 2012a) and numerical simulations (Cagnoli and Piersanti, 2015), we computed an apparent coefficient of friction equal to the ratio of the vertical drop  $h$  of the centre of mass of the granular mass to its horizontal displacement  $l$ :

$$\mu_A = \frac{h}{l}. \quad (13)$$

These horizontal and vertical distances are measured from the centre of mass of the granular body behind the gate before release to the centre of mass of the final deposit of the flow proper. We compare  $\mu_A$  and  $\mu_B$  by plotting them in the same figure versus the following parameter:

$$\chi = \frac{V^{1/3} \delta}{L w}, \quad (14)$$

where  $L$  is the length of the deposit. Scaling parameter  $\chi$  was introduced by Cagnoli and Piersanti (2017) to quantify the functional dependence of flow mobility on grain size, flow volume and channel width.

## 4. Results

The linear correlation coefficient  $r$  (Taylor, 1997) is computed for all the  $D$  versus  $\psi$  plots (Figs. 5, 6, 7 and 8). Table 4 shows the percentage probability that 16 measurements for each of two uncorrelated variables give these  $r$  values (the number of flows examined here is 16). According to Taylor (1997), a correlation is called highly significant if the probability is  $< 1\%$ , whereas a correlation is called significant if the probability is  $\leq 5\%$  and  $> 1\%$ .

Fig. 5 shows the  $D$  versus  $\psi$  plots of the total pressures exerted by the granular flows on the three measurement areas. The linear correlation coefficient  $r$  is higher for areas one (0.82) and two (0.83) and it is smaller for areas three (0.53). According to the probability values in Table 4, the linear correlations between  $D$  and  $\psi$  are highly

significant in areas one and two, whereas the linear correlation is significant in area three. An interesting observation is that the slope of the fitting straight line decreases from area one to area two and from area two to area three.

Fig. 6 shows the  $D$  versus  $\psi$  plots of the normal pressures exerted by the granular flows on the three measurement areas. The linear correlation coefficient  $r$  is higher for areas one (0.80) and two (0.82) and it is smaller for area three (0.494). According to the probability values in Table 4, the linear correlations between  $D$  and  $\psi$  are highly significant in areas one and two, whereas, for area three, the probability (5.2%) is only marginally higher than the 5% value with which a correlation is considered significant. The slope of the fitting straight line decreases from area one to area two and from area two to area three.

Fig. 7 shows the  $D$  versus  $\psi$  plots of the parallel pressures exerted by the granular flows on the three measurement areas. The linear correlation coefficient  $r$  is higher for areas one (0.88) and two (0.83) and it is smaller for area three (0.56). According to the probability values in Table 4, the linear correlations between  $D$  and  $\psi$  are highly significant in areas one and two, whereas the linear correlation is significant in area three. The slope of the fitting straight line decreases from area one to area two and from area two to area three.

Fig. 8 shows the  $D$  versus  $\psi$  plots of the transversal pressures exerted by the granular flows on the three measurement areas. The linear correlation coefficient  $r$  is higher in area one (0.67) than in area two (0.55) and in area three (0.52). According to the probability values in Table 4, the linear correlations between  $D$  and  $\psi$  is highly significant in area one, whereas the linear correlations are significant in areas two and three. The slope of the fitting straight line is larger in area one than in areas two and three.

In Fig. 9, we plot the values of  $\mu_A$  versus  $\chi$  which display a significant linear correlation. These  $\mu_A$  and  $\chi$  values were computed by Cagnoli and Piersanti (2017). Fig. 9 reveals also that, on the contrary, the values of  $\mu_B$  and  $\chi$  are not correlated.

## 5. Discussion

The numerical simulations discussed in this paper confirm the effects of grain size and flow volume on the scaled basal pressure fluctuation  $D$  that we observed in laboratory experiments (Cagnoli and Romano, 2012b). This result confirms the trustworthiness of the 3-D discrete element modeling. In both numerical simulations and laboratory experiments,  $D$  is directly proportional to the square of grain size and it is inversely proportional to the cube root of flow volume. The novel contribution of this paper is that: 1) this is valid not only for  $D$  computed with the normal pressures but also for  $D$  computed with the total, parallel and transversal pressures as well (Figs. 5, 6, 7 and 8) and 2) this is valid irrespective of the value of the channel width.

Therefore, the numerical simulations confirm that the larger the grain size, the larger the scaled basal pressure fluctuation  $D$  (Figs. 5, 6, 7 and 8). This effect of grain size is strong because it is the square of grain size that enters parameter  $\psi$ . This is due to the fact that (all the other features being the same, including the flow mass), the larger the grain size, the smaller the number of particles in the flow, so that particles agitation that is generated in contact with the boundary surfaces (both the lateral and the basal ones) propagates deeper within the flow. This is represented in Eq. (7) by: 1) the inverse proportionality between  $D$  and  $\Gamma$ , where  $\Gamma$  is an increasing function of the total number of particles in the flow (Eq (10)) and 2) the inverse proportionality between  $D$  and  $\Omega$ , where  $\Omega$  is an increasing function of the number of particles that fits the channel width (Eq. (11)). This means that, with larger grain size, there is a relatively larger particle agitation per unit of flow mass. This explanation is demonstrated by the experimental measurements (Cagnoli and Romano, 2012b) and the numerical simulations (Cagnoli and Piersanti, 2015).

The numerical simulations confirm also that the larger the flow volume, the smaller the scaled basal pressure fluctuation  $D$  (Figs. 5, 6, 7 and 8). This is so because (all the other features the same, including the grain size), the larger the flow volume, the larger the number of particles in the granular flow, so that particle agitation that is generated in contact with the boundary surfaces penetrates relatively less inside the flow. This is represented in Eq. (7) by the inverse proportionality between  $D$  and  $\Gamma$ , where  $\Gamma$  is an increasing function of the total number of particles in the flow (Eq. (10)). This means that, with larger volumes, there is a smaller particle agitation per unit of flow mass. This explanation is demonstrated by the experimental measurements (Cagnoli and Romano, 2012b) and the numerical simulations (Cagnoli and Piersanti, 2015).

The laboratory experiments showed that the scaled basal particle agitation  $D$  is correlated with the agitation of the particles measured on the top surface of the flows by means of a video camera (Cagnoli and Romano, 2012b). This is so precisely because particle agitation is generated in contact with the subsurface (where it is larger) and from there it propagates upward (where particles are relatively less agitated). Flows with the larger volume and or the finer grain size are denser because of the smaller particle agitation whereas flows with the smaller volume and or the larger grain size are more dilated because of the increased particle agitation. The so-called plugs are thus more likely to occur in flows with larger volumes and or finer grain size. The energy dissipation that affect flow mobility and that is due to particle agitation does not occur only at the base but also inside the granular flow.

An important novel result demonstrated in this paper is that the basal pressure fluctuation  $D$  is inversely proportional to the channel width. This is true for the total pressure as well as its normal, parallel and transversal components (Figs. 5, 6, 7 and 8). Therefore, all the other features being the same, the larger the channel, the smaller the particle agitation per unit of flow mass. This is due to the fact that particle agitation is generated also in contact with the sidewalls (besides the subsurface) and, the larger the distance between the sidewalls, the smaller the penetration of this agitation within the flow. This is represented in Eq. (7) by the inverse proportionality between  $D$  and  $\Omega$ ,

where  $\Omega$  is an increasing function of the number of particles that fit the distance between the inclined sidewalls (Eq. (11)).

The data obtained with the numerical simulations (Figs. 5, 6, 7 and 8) are more scattered than those obtained in the laboratory experiments (Cagnoli and Romano, 2012b). One possible explanation of the larger scatter is that, in the numerical simulations, the extent of the measurements areas in proportion to the grain size is larger than that in the laboratory experiments. In the numerical simulations, the measurements areas are squares with sides equal to 6, 10, 16 and 26 mm with respect to grain sizes equal to 1, 1.5 or 2 mm. In the laboratory experiments, the load cell plate is a disc 5 mm in diameter and the grain size ranges between 0.5 and 3 mm. This results in pressure values  $P_i$  in the numerical simulations, that are more likely due to more than one collision at the same time. A scatter increase could also be due to the conservative criterion we use to remove the pressure values of the saltating particles at the front and at the back of the flows. This conservative criterion results in  $D$  values estimated by including also some pressure values generated by the saltating particles. In spite of this, all the linear correlations between  $D$  and  $\psi$  (Table 4) are either significant or highly significant (only in Fig. 6c, the probability is slightly higher than the conventional threshold value).

The transversal pressure has linear correlation coefficients that, in areas one and two, are significantly smaller than those of the other pressures and, in area three, are virtually as small as those of the other pressures (Table 4). This is accompanied by the fact that, on all three measurement areas, the transversal pressures have values smaller than those of the normal and parallel pressures. On average in the 16 flows, the mean transversal pressures are approximately 19%, 16% and 12% of the sum of the means of the normal and parallel pressures in areas one, two and three, respectively. This suggests that the process that generates the basal forces gives more prominence to those on the plane containing the flow direction, i.e. in the normal and parallel directions.

Eq. (7) is important because it links the basal pressures with grain size, flow volume and channel width. The increase of particle agitation as grain size increases (Figs. 5, 6, 7 and 8) is compatible with the decrease of the mobility of the center of mass as grain size increases that was observed in laboratory experiments (Cagnoli and Romano, 2012a) and numerical simulations (Cagnoli and Piersanti, 2015; Cagnoli and Piersanti, 2017). Also the decrease of particle agitation as the channel width increases is compatible with the larger mobility of the centre of mass as channel width increases computed by Cagnoli and Piersanti (2017). This is so because an increase of particle agitation causes an increase of energy dissipation per unit of travel distance.

Similarly, we would expect an increase of mobility as flow volume increases, because of the decrease of particle agitation as flow volume increases (Figs. 5, 6, 7 and 8). In fact, both laboratory experiments (Cagnoli and Romano, 2012a) and numerical simulations (Cagnoli and Piersanti, 2015; Cagnoli and Piersanti, 2017) showed a decrease of the mobility of the center of mass as flow volume increases. This is due to the fact that, during deposition on a slope with a gradual (Cagnoli and Piersanti, 2015) or an abrupt (Okura et al., 2000) change of its inclination angle, a deposit accretes backward and the

larger the volume, the larger this backward accretion and consequently the larger the backward migration of the center of mass. Therefore, the increase of mobility of the center of mass that we would expect from a reduced particle agitation per unit of flow mass as flow volume increases is canceled out by this backward accretion.

The decrease of the mobility of the center of mass as flow volume increases does not contradict the larger mobility of the flow front as flow volume increases described by Scheidegger (1973), because these are two distinct phenomena. The increase of the mobility of the flow front as flow volume increases is visible in our system as well (Cagnoli and Romano, 2012a) and it is due to the fact that the planimetric area inundated by a flow is proportional to a power of the flow volume (Griswold and Iverson, 2008) so that, in a channel, the larger the flow volume, the longer the longitudinal spreading of the flow and its deposit (Davies, 1982; D'Agostino et al., 2010).

Importantly, the straight lines fitting the data in the plots of  $D$  versus  $\psi$  (Figs. 5, 6, 7 and 8) intercept the vertical axis above the origin because the pressure fluctuation and, thus, particle agitation, is always different from zero at the base of a granular flow. This explains why parameter  $\mu_B$  and parameter  $\chi$  are not correlated (Fig. 9). Parameter  $\mu_B$  is the ratio of the parallel to the normal pressures exerted at the base by a rigid object (such as a brick) that slides. In granular flows, instead, the basal interactions with the subsurface consist of particle collisions (Cagnoli and Romano, 2012b). In Fig. 9, it is therefore parameter  $\mu_A$  that is correlated with parameter  $\chi$ , because  $\mu_A$  describes the mobility of the center of mass of a granular flow and  $\chi$  is the product of the flow characteristic numbers of particles (Cagnoli and Piersanti, 2017).

Interestingly, the slope of the fitting straight lines decreases from area one to area two and from area two to area three, whereas their intercept with the vertical axis is always at  $D \sim 2$  (Figs. 5, 6, 7 and 8). Therefore, in the more distal position, the flows with larger  $\psi$  values have smaller particle agitation  $D$ . This is so because the flows in the more distal positions have dissipated so much of their energy (in area three they are about to stop) that particle agitation has decreased in relative terms even if the grain size is still large and or the flow volume is still small and or the channel width is still small. The different flows have thus more different particle agitation  $D$  in a more proximal area than where the flows are about to stop in a more distal place. The coefficients of linear correlation for all pressures are also significantly smaller in area three than in areas one and two (Table 4), precisely because Eq. (7) pertains to a collisional regime which is less developed near deposition where the energy of the flows is almost completely exhausted.

## 6. Conclusions

We advance here a functional relation that links the pressures exerted on the subsurface by flows of angular rock fragments and three quantities that affect flow mobility: grain size, flow volume and the channel width. This relation has been obtained by means of 3-D discrete element modeling and, as far as the grain size and the flow volume are concerned, we validated it in laboratory experiments where a load cell measured the normal pressures. However, our calculations in this paper show the validity

of this relationship not only for the normal pressures but also for the pressure components along the flow-parallel and the flow-transversal directions and thus for the total basal pressures as well. The original contribution of these numerical simulations is also the relation between the basal pressures and the channel width obtained by comparing flow data in four different channels whose construction and use in laboratory experiments would have been truly demanding.

This functional relation consists of a linear correlation between the dimensionless basal pressure fluctuation  $D$  and the scaling parameter  $\psi$  which contains, at the numerator, the grain size squared and, at the denominator, the cube root of the flow volume multiplied by the channel width. According to this equation, the agitation of the particles per unit of flow mass increases as grain size increases and it decreases as flow volume increases and as channel width increases (in each case, all the other features the same). Since parameter  $\psi$  can be expressed as the product of the reciprocal of two characteristic numbers of fragments which are, as such, dimensionless, this relation is valid at any scale either in the laboratory or in nature. The granular flows in our simulations are meant to model rock avalanches and pyroclastic flows which travel within channels on the flanks of mountains and volcanoes. Particle agitation and basal pressures are important because they affect flow mobility and therefore the hazards that the geophysical flows are responsible for.

## References

- Abe, S., Mair, K., 2009. Effects of gouge fragment shape on fault friction: New 3D modelling results. *Geophys. Res. Lett.* 36, L23302, doi:10.1029/2009GL040684.
- Cagnoli, B., Piersanti, A., 2015. Grain size and flow volume effects on granular flow mobility in numerical simulations: 3-D discrete element modeling of flows of angular rock fragments. *J. Geophys. Res. Solid Earth* 120, 2350-2366. doi: 10.1002/2014JB011729.
- Cagnoli, B., Piersanti, A., 2017. Combined effects of grain size, flow volume and channel width on geophysical flow mobility: 3-D discrete element modeling of dry and dense flows of angular rock fragments. *Solid Earth* ...
- Cagnoli, B., Romano, G.P., 2012a. Effects of flow volume and grain size on mobility of dry granular flows of angular rock fragments: A functional relationship of scaling parameters. *J. Geophys. Res.* 117 (B02207). doi:10.1029/2011JB008926.
- Cagnoli, B., Romano, G.P., 2012b. Granular pressure at the base of dry flows of angular rock fragments as a function of grain size and flow volume: A relationship from laboratory experiments. *J. Geophys. Res.* 117 (B10202). doi:10.1029/2012JB009374.
- D'Agostino, V., Cesca, M., Marchi, L., 2010. Field and laboratory investigations of runout distances of debris flows in the Dolomites (Eastern Italian Alps). *Geomorphology*, 115, 294-304.
- Davies, T.R., 1982. Spreading of rock avalanche debris by mechanical fluidization. *Rock Mech.* 15, 9-24.
- Dym, C.L., 2004. *Principles of Mathematical Modeling*. Elsevier Academic Press, San Diego, California.

- Griswold, J.P., Iverson, R.M., 2008. Mobility statistics and automated hazard mapping for debris flows and rock avalanches. U.S. Geological Survey Scientific Investigations, Report 2007-5276.
- Hertz, H., 1882. Über die Berührung fester elastischer Körper. *J. Reine Angewandte Mathematik* 92, 156-171.
- Iverson, R.M., Logan, M., LaHusen, R.G., Berti, M., 2010. The perfect debris flows? Aggregated results from 28 large-scale experiments. *J. Geophys. Res.* 115 (F03005). doi: 10.1029/2009JF001514.
- Kang, C., Chan, D., Su, F., Cui, P., 2016. Runout and entrainment analysis of an extremely large rock avalanche – a case study of Yigong, Tibet, China. *Landslides*, doi:10.1007/s10346-016-0677-7
- Lambe, T.W., Whitman, R.V., 1969. *Soil Mechanics*, John Wiley and Sons, New York.
- McCoy, S.W., Tucker, G.E., Kean, J.W., Coe, J.A., 2013. Field measurement of basal forces generated by erosive debris flows. *J. Geophys. Res. Earth Surf.* 118, 1-14, doi:10.1002/jgrf.20041.
- Mindlin, R.D., 1949. Compliance of elastic bodies in contact. *J. Appl. Mech.* 16, 259-268.
- Mindlin, R.D., Deresiewicz, H., 1953. Elastic spheres in contact under varying oblique forces. *J. Appl. Mech.* 20, 327-344.
- Okura, Y., Kitahara, H., Sammori, T., Kawanami, A., 2000. The effects of rockfall volume on runout distance. *Eng. Geology* 58, 109-124.
- Peng, B., 2000. *Rockfall Trajectory Analysis: Parameter Determination and Application*. M.S. thesis. University of Canterbury, Christchurch, New Zealand.
- Saucedo, R., Macías, J.L., Bursik, M.I., Mora, J.C., Gavilanes, J.C., Cortes, A., 2002. Emplacement of pyroclastic flows during the 1998-1999 eruption of Volcán de Colima, México. *J. Volcanol. Geotherm. Res.* 117, 129-153.
- Scheidegger, A.E., 1973. On the prediction of the reach and velocity of catastrophic landslides. *Rock Mech.* 5, 231-236.
- Taylor, J.R., 1997. *An Introduction to Error Analysis*. University Science Books, Sausalito, California.
- Yohannes, B., Hsu, L., Dietrich, W.E., Hill, K.M., 2012. Boundary stresses due to impacts from dry granular flows. *J. Geophys. Res.* 117, F02027, doi:10.1029/2011JF002150.
- Zhang, M., Yin, Y., 2013. Dynamics, mobility-controlling factors and transport mechanisms of rapid long-runout rock avalanches in China. *Eng. Geol.* 167, 37-58.

## FIGURES

**Fig.1.** Longitudinal and transversal (in the inset) profiles of all the channels used in the numerical simulations. Quantity  $w$  is the channel width and quantity  $\theta$  is the sidewall inclination. CM stands for center of mass.

**Fig. 2.** Bird's-eye view of a granular flow traveling downslope along a channel in a numerical simulation. The grain size  $\delta$  is 1 mm, the flow mass is 26 g and the channel width  $w$  is 6 mm. The color bar shows the particle velocities. The time in seconds is that elapsed after the removal of the gate. The particles moving in front of the denser part of the flow are those that will form the distal spray of isolated particles when deposited. The flow direction in this figure is downward.

**Fig. 3.** The three particle shapes used in the numerical simulations with the sets of inscribed spheres.

**Fig. 4.** Example of a time series of total pressure values  $P_i$  exerted on the channel surface by a granular flow (the time step is 0.01 sec). These pressures are exerted on area one by a granular flow whose mass is 39 g and whose grain size  $\delta$  is 1 mm. The channel width  $w$  is equal to 26 mm. When the flow has not arrived yet or it has already passed by the measurement area, the pressure values are zero.

**Fig. 5.** Plots of scaling parameters  $D$  versus  $\psi$ , where  $D$  is computed for the total pressures. The three plots a), b) and c) are those of data in measurement area one, two and three, respectively. Quantity  $r$  is the linear correlation coefficient whose value is shown in each plot.

**Fig. 6.** Plots of scaling parameters  $D$  versus  $\psi$ , where  $D$  is computed for the normal pressures. The three plots a), b) and c) are those of data in measurement area one, two and three, respectively. Quantity  $r$  is the linear correlation coefficient whose value is shown in each plot.

**Fig. 7.** Plots of scaling parameters  $D$  versus  $\psi$ , where  $D$  is computed for the parallel pressures. The three plots a), b) and c) are those of data in measurement area one, two and three, respectively. Quantity  $r$  is the linear correlation coefficient whose value is shown in each plot.

**Fig. 8.** Plots of scaling parameters  $D$  versus  $\psi$ , where  $D$  is computed for the transversal pressures. The three plots a), b) and c) are those of data in measurement area one, two and three, respectively. Quantity  $r$  is the linear correlation coefficient whose value is shown in each plot.

**Fig. 9.** Apparent coefficients of friction  $\mu_A$  and  $\mu_B$  plotted versus scaling parameter  $\chi$ . These three plots are those of data in measurement area one, two and three, respectively. Parameter  $\mu_A$  is correlated with  $\chi$ , parameter  $\mu_B$  is not.

**Table 1**

Characteristics of channels (ramps and curved chutes) and flows.

Channel Width $w$ mm	Total Flow Mass g	Grain Size $\delta$ mm
6	8.9	1
6	13	1
6	26	1, 1.5, 2
10	29	1, 1.5, 2
16	33	1, 1.5, 2
26	39	1, 1.5, 2
26	93	2
16	68	2

**Table 2**

Physical properties of materials.

	Particles	Ramps and Chutes	Gates
Poisson's Ratio	0.19	0.35	0.36
Shear Modulus (Pa)	2.38e+10	6.85e+09	25e+09
Density (kg/m <sup>3</sup> )	2700	2580	2700

**Table 3**

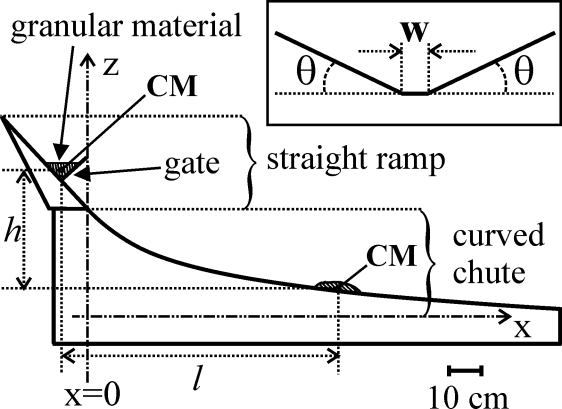
Values of properties governing particle-particle, particle-channel and particle-gate interactions. A channel comprises the straight ramp and the curved chute.

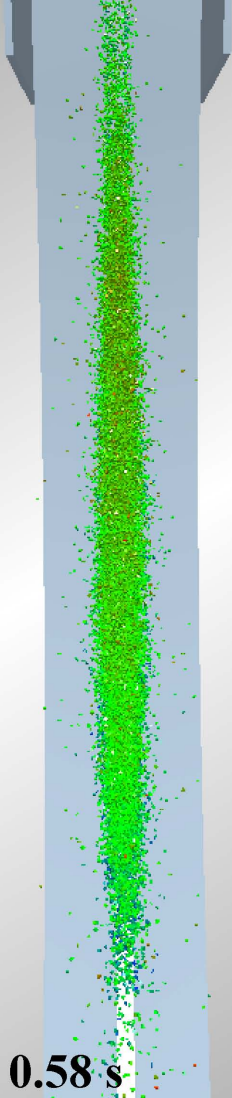
	Particle-Particle	Particle-Channel	Particle-Gate
Coefficient of Restitution	0.49	0.3	0.53
Coefficient of Static Friction	0.45	0.9	0.1
Coefficient of Rolling Friction	0.035	0.07	0.07

**Table 4**

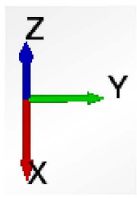
Percentage probabilities of linear correlation coefficients  $r$  of 16 values for each of two uncorrelated variables (Taylor, 1997).

	Area One		Area Two		Area Three	
	$r$	Prob	$r$	Prob	$r$	Prob
Total Pressures	0.82	0.01	0.83	<0.01	0.53	3.5
Normal Pressures	0.80	0.02	0.82	0.01	0.494	5.2
Parallel Pressures	0.88	<0.01	0.83	<0.01	0.56	2.4
Transversal Pressures	0.67	0.45	0.55	2.73	0.52	3.9





Speed (m/s)



18 mm

0.58 s

